Italian Journal of Engineering Geology and Environment
www.ijege.uniroma1.it

ENGINEERING GEOLOGICAL FACTORS AFFECTING LOESS CAVES SUSCEPTIBILITY MAPPING IN GORGAN PLAIN, GOLESTAN PROVINCE, NORTHEASTERN IRAN

Seddighe ZALAGHAIE(*), Mojtaba HEIDARI (*),
Mohammad Reza NIKUDEL(**) & Bahman SAEDI (*)

(*) *Bu-Ali Sina University, Department of Geology, Mahdieh St., Hamedan, Iran*
(**) *Tarbiat Modares University, Department of Engineering Geology, Al Ahmad St., Tehran, Iran*
Corresponding author: moj.heidari@basu.ac.ir

EXTENDED ABSTRACT

Il loess è un deposito quaternario ampiamente diffuso nelle regioni aride e semiaride. I suoli loess hanno una struttura aperta con elevata sensibilità all'acqua e comprimibilità. Di conseguenza, questo tipo di suolo può determinare gravi problemi ambientali, determinando cedimenti causati da pioggia o da irrigazione, l'innalzamento della falda freatica e innescare fessurazioni in terreni interessati da infiltrazioni (Xu *et alii*, 2015; Peng *et alii*, 2016). Ciò determina spesso gravi conseguenze economiche e sociali con perdite di vite umane, la distruzione del suolo e il danneggiamento dei campi agricoli, il deterioramento delle infrastrutture, quali gasdotti e oleodotti e l'alterazione delle vie di trasporto. Gli approcci per la zonazione del rischio possono essere suddivisi a grandi line in qualitativi (metodi basati sulla conoscenza) e quantitativi (metodi basati sui dati). I metodi quantitativi sono basati su procedure statistiche. Queste procedure sono state generalmente utilizzate nella preparazione delle mappe di suscettibilità alle frane, sebbene questi metodi possano essere utilizzati anche nelle mappe di suscettibilità di grotte di loess. E' stata eseguita un'analisi della suscettibilità alle frane mediante modelli statistici che utilizzano procedure bivariate o multivariate e sono state studiate le performance e i limiti di una combinazione degli approcci attuali. Nello studio della zonazione di suscettibilità di grotte di loess sono stati utilizzati modelli di predizione statistica e probabilistica. Pertanto, l'obiettivo principale di questo studio è affrontare il problema della validazione dei modelli di suscettibilità di grotte di loess nella provincia del Golestan (Iran nordorientale), precisamente nella pianura di Gorgan. Vengono quindi valutati i fattori che ne influenzano la loro presenza e, infine, condotta la mappatura della suscettibilità delle grotte di loess, confrontando la *performance* di tre modelli, *Density Area (DA), Information Value (IF) e Frequency Ratio (FR)* .

Ampie aree dell'Iran settentrionale sono state ricoperte da loess, formando una delle parti più meridionali della cintura eurasiatica del loess. Questa cintura di loess circonda il Medio Oriente e copre Tagikistan, Kazakistan e Turkmenistan (Keshavarzi, 2014). La ricerca è stata condotta nell'altopiano iraniano di Loess, identificato da depositi di loess da sud a nord della provincia del Golestan, tra 38.15 N e 36.30 N di latitudine e 54.00 E e 56.00 E di longitudine. Sulla base delle caratteristiche geotecniche e sedimentologiche, il loess di questa provincia si suddivide in tre zone: I (loess argilloso), II (loess limoso) e III (loess sabbioso). L'allontanamento dal sito di origine e la diminuzione dell'energia eolica hanno disperso i suoli di loess e i fattori che modificano la struttura del suolo sono stati differenziati in tre aree con climi diversi con piovosità media annua variabile da 200 a 750 mm/anno da nord a sud della provincia del Golestan.

Informazioni come mappe geologiche e topografiche, eventi storici di formazione di grotte di loess, analisi di laboratorio, interpretazioni di immagini satellitari e indagini sul campo utilizzando il Global Positioning System (GIS) sono state conisderate come variabili dipendenti. Per prevedere le aree a potenziale sviluppo di grotte di loess, sono stati prodotti e digitalizzati in ambiente ArcGIS come fattori determinant l'incidenza di grotte di loess (variabili indipendenti), gli strati informativi includenti: geologia, pendenza, assetto, elevazione, erosione, precipitazioni, uso del suolo, tipo di suolo, classificazione del suolo USDA, distanza da strade, distanza da fiumi e predisposizione ai collassi. E' stato studiato l'effetto di tutti i fattori proposti e l'ubicazione di ciascuna grotta di loess è stata documentata mediante l'applicazione del GIS ai dati basati su sopralluoghi in campo. La mappatura basata sui dati di campo è stata supportata dall'interpretazione dei dati digitali raccolti da un veicolo aereo senza pilota (UAV), il quadricottero DJI Phantom 4 Pro con una fotocamera DJI FC6310. Il software ArcGIS 10.2.2 è stato utilizzato per tracciare i record in formato raster e per calcolare i parametri fisici e meccanici che regolano la dispersione delle grotte in loess, abbiamo preparato campioni di blocchi indisturbati provenienti da 62 punti nelle zone I, II e III. Dopo la pulizia, tutti i campioni sono stati posti in scatole da 20 × 20 × 20 cm e trasferiti al laboratorio di geologia applicata. Nelle mappe delle classi dei fattori determinanti e pesati per Information Value, Density Area e Frequency Ratio, lo studio è stato condotto in ArcGIS utilizzando un'analisi basata sui pixel. La dimensione di ogni pixel è 30 m×30 m, con griglia quadrata. Inoltre, dalla somma algebrica delle mappe ponderate relative ai breakpoint della curva di frequenza sono state derivate mappe di zonazione di pericolosità per grotte di loess. Infine, le curve ROC sono state valutate con l'ausilio della capacità predittiva o della competenza delle mappe di suscettibilità, in un grafico che fissa la relazione tra Sensibilità e specificità del modello su una serie di soglie per un risultato positivo. La determinazione dell'AUC consente la valutazione quantitativa della capacità predittiva complessiva dei modelli di suscettibilità.

IJEGE, 1 (2022): 15-30, DOI: 10.4408/IJEGE.2022-01.O-02
E-ISSN 2035-5688 | ISSN 1825-6635 / ©*Author(s)*

ABSTRACT

Loess cave is one of the geological hazards in the Loess Plateau of northeast Iran, in the Gorgan plain. In total, 697 caves were mapped, and an inventory map was prepared. Due to the importance of geo-environmental and soil properties in the development of loess caves, six independent variables, including joint density, land use, soil type, collapse sensitivity, self-weight collapse coefficient, and surface water distance, were designed for modeling the caves susceptibility in the GIS software. Loess cave susceptibility maps were constructed using Density Area (DA), Information Value (IF), and Frequency Ratio (FR) methods in a GIS environment. Loess cave susceptibility map obtained from three models was compared using Relative Operating Characteristic (ROC) and Area Under Curve (AUC). The area under the curve analysis was used to evaluate model compatibility and predictability. The equal interval classification method classified the study area into five ordinal categories, i.e., very low, low, moderate, high, and very high. AUC of the IF model was 0.727. The values of AUC for DR and the FR models were similar and equal to 0.725. Therefore, the loess cave susceptibility maps of Golestan Province is valuable for decision-maker in loess cave-prone area.

Keywords*: loess cave zonation, information value, density area, frequency ratio, validation*

ARTICLE HIGHLIGHTS

- Preparing the loess cave susceptibility map in Golestan Province utilizing the bivariate statistical approach.
- The concept of collapse sensitivity was calculated with the laboratory tests in detail.
- Performing soil mechanics laboratory tests on loess soils to determine the Ic, collapse speed, and collapse sensitivity (Is).
- Preparing the joint density map using the Global Positioning System (GIS), compass, aerial photographs, and satellite images.
- Evaluation and comparison of FA, DR, and IF models.

INTRODUCTION

Loess is a Quaternary deposit that is broadly spread in arid and semiarid regions. Loess soils have an open structure, high water sensitivity, and collapsibility properties. As a result, this specific loess inappropriately can pose severe environmental difficulties, such as subsidence caused by rain or irrigation, the rising water table, and ground fissures affected by seepage (Xu *et alii*, 2015; Peng *et alii*, 2016). Water seepages show strong water sensitivity of disintegration, dissolution, liquefaction, creep, and sliding. Research on the water sensitivity of loess and its special-temporal distribution has a practical significance in guiding the engineering constructions in the unsaturated loess area. Based on the theory of unsaturated loess, the concept of suction stress is introduced to explain the water sensitivity of loess. The essence of water sensitivity is that the suction stress decreases with increased water content, and the different deformation behaviors will occur under different boundary conditions. Loess collapse is one of the most severe environmental problems in Golestan Province in NE, Iran. Several geo-hazards and engineering challenges occur in Golestan Province's loess, such as landslides, gully, subsidence, and loess cave. All of these landscapes are created by high collapsibility (Salehi, 2011). They often have severe environmental and economic consequences such as human loss, soil destruction and damaging agricultural fields, undermining infrastructure, gas and oil pipelines, and altering transportation corridors (Fig.1).

Despite numerous studies on slope instability (Ghorbanzadeh *et alii*, 2021; Ghobadi *et alii*, 2017; Pourghasemi *et alii*, 2019) and gullies (Amiri *et alii*, 2019; Karimi Nejad *et alii*, 2019), unfortunately, little research has been done on the factors affecting the occurrence of loess cave and its zoning in Golestan province. Caves, in non-karstic landscapes, refer to the formation of linear voids by the collapse of the soil surface due to the wetting of loess soils. It is prevalent in different regions. Loess cave results from hydro-mechanical, gravitational, biological, and physic-chemical destruction of the soil. Loess collapse causes the formation of landforms that are very reminiscent of the typical karsts (dips, loess caves, gullies, circuses, tunnels, etc.)(Lavrusevich, 2019). Under natural conditions, the loess cave develops slowly and affects large areas. There is no single meaning of the term "Loess cave," described in detail and reviewed by Peng *et alii* (2017). Richthofen earliest defined this process in China in 1877 (von Richthofen, 1877). Later this course was called under a multiplicity of names: subterranean erosion (Fuller, 1922), piping (Fletcher & Carroll, 1948), and pseudokarst (Halliday, 2007). The engineering geological problems of loess have attracted extensive research in past decades. Loess-associated geo-hazards bring about severe infrastructure loss and soil loss (Zgłobicki *et alii*, 2016; Bernatek-Jakiel *et alii*, 2017). Therefore, scientists must predict and research the spatial occurrence of the loess cave. Land managing denotes the most robust tool to contrast the opposing effects of loess cave. A strategic contribution comes from loess cave susceptibility mapping. This mapping offers a given area into regions of different grades of susceptibility to the phenomenon, which is essential for exact land-use development. Several techniques are powerfully suggested to produce comprehensive and consistent susceptibility maps. GIS is critical in susceptibility mapping as it permits easy management and processing of regional data, which is central of susceptibility evaluation processes (Chen *et alii*, 2011).

The approaches for risk zoning can be broadly classified as

Fig. 1 - a) Abundance of loess caves on Kalaleh-Maraveh Tappeh road b) A loess cave developed near the Cheshmehli village road c) Loess caves along the power transmission line around Maraveh Tappeh d) Typical landslide developed on the loess plateau in Golestan Province e) Differential settlement of residential building in Feraghi city, and Bending of gas supply pipe of houses in Feraghi city due to loess collapse

qualitative (knowledge-driven methods) and quantitative (data-driven methods). Data-driven methods are quantitatively based on statistical procedures (Bai *et alii*, 2010; Lara & Sepulveda, 2010). These procedures have been used generally in preparing landslide susceptibility maps, although these methods can also be used in susceptibility maps of loess caves. Landslide susceptibility analysis by statistical models using bivariate or multivariate procedures has been done and studied the performance and restrictions of a combination of current approaches (Romer & Ferentinou, 2016; Li *et alii*, 2017; Abedini *et alii*, 2017; Hadmoko *et alii*, 2017). In the study of loess cave susceptibility zonation, statistical and probabilistic prediction models are used.

Therefore, the main objective of this study is to deal with the issue of validating loess cave susceptibility models in Golestan province. The Gorgan plain is highly prone to loess caves, therefore, in this study, we evaluate the factors affecting their occurrence and, finally, loess cave susceptibility mapping. This study assessed the performance of three Density Area (DA), Information Value (IF), and Frequency Ratio (FR) models in the loess cave susceptibility map.

STUDY AREA AND GEOLOGICAL SETTING

Large areas in northern Iran have been covered by loess, forming one of the southernmost parts of the Eurasian loess belt. This loess belt surrounds the Middle East and covers Tajikistan, Kazakhstan, and Turkmenistan (Keshavarzi, 2014). The research was performed in the Iranian Loess Plateau, identified by loess deposits from the south to the north of the Golestan Province, between 38.15 N and 36.30 N latitude and 54.00 E and 56.00 E longitude (Fig. 2).

Fig. 2 - Location map of the study area

This province is located northeast of Iran and on the south-eastern shore of the Caspian Sea, which is part of the so-called Kopeh Dagh structural zone (Karimi *et alii*, 2009). Geologically, it lies within the northern margin of central Iran on the southern edge of the Touran Plate (Eftekharnejad & Behroozi, 1991). The thickness of the Golestan loess deposits decreases from northeast to southwest and covers more than 17 % (388,000) hectares of the province area (Feiznia, 2005). Based on geotechnical and sedimentology characteristics, the loess of this province is extended in the three zones I (clay loess), II (silty loess), and III (sandy loess).

Being away from their origin and decreased wind energy has dispersed loess soils, and the factors changing the soil's structure were differentiated in three areas with different climates. Based on the arid-humid climate classification De Martone (De Martonne ,1926), the province is divided into climates to 5 Climate zones: Semiarid, Mediterranean, Semi-humid, Wet, and Very Wet. In general, most of the area is in a semiarid environment. Average annual rainfall ranges from 200 to 750 mm/year from north to south of Golestan Province.

METHODOLOGY

Information such as geological and topographic maps, historical loess cave events, laboratory analysis, satellite image interpretations, and field investigations using the Global Positioning System (GIS) was prepared as dependent variables. To predict the loess cave potential areas, the information layers, including geology, slope, aspect, elevation, erosion, precipitation, land use, soil type, USDA Soil Taxonomy, road distance, river distance, and sensitivity collapse, were produced and digitized as determining factors in loess cave incidence (independent variables) in ArcGIS environment. The effect of all the proposed factors was investigated. Due to the lack of influence of some primary selection factors on the occurrence of loess caves, they have been excluded from the final analysis. The variables were selected based on previous studies (Kariminejad *et alii*, 2020; Zhang *et alii*, 2018).

According to the primary hypothesis, future geo-environmental factors will happen under similar conditions (Lee & Talib, 2005). The location of each loess cave was documented by applying GIS based on field visits. The field-based mapping was patronaged by interpreting digital data gathered by an unmanned aerial vehicle (UAV), the DJI Phantom 4 Pro quadcopter with a DJI FC6310 camera. ArcGIS 10.2.2 software was employed to plot the records in raster format.

To calculate the physical and mechanical parameters governing the scattering of loess caves, we prepared undisturbed block samples from 62 points in Zones I, II, and III. After waxing, all samples were placed in 20 × 20 × 20 cm boxes and transferred to the engineering geology laboratory. In addition, an odometer test was carried out based on (ASTMD 5333-03 2003) standard. Seven samples with a diameter of 75 mm and a height of 20 mm were set up from each site to determine the Ic (collapse coefficient), collapse speed, self-weight collapse coefficient, and initial pressure required for collapse. The samples were exposed to pressures of 25, 50, 100, 200, 400, 800, and 1600 Kpa. In the standard method, the collapse coefficient of soils is determined at a pressure of 200 Kpa. However, in the current study, the collapse coefficient of soils was determined under different pressures. Loading stages are 25, 50, 100, 200, 400, and 800 Kpa, respectively. The deformation at each step of loading was read at intervals of 0.1, 0.25, 0.5, 1, 2, 4, 6, 9, 12, 16, 20, 25, 30, 45, and 60 min. Then it was continued at intervals of 30 min until reaching a steady state (deformation value less than 0.01 mm per hour). Laboratory test outcomes show in table 1.

In classes of determining factor maps and weighted by Information Value, Density Area, and Frequency Ratio, the study was conducted utilizing pixel-based analysis in ArcGIS. The size of each pixel is 30 m×30 m, a square grid. In addition, loess cave hazard zonation maps were acquired from the algebraic sum of weighted maps concerning breakpoints of the frequency curve.

Soil Type	sample Number	w %	n%	CaCO3%	LL%
clay Loess	S-M1	3.89	46.20	27.17	51.8
	S-M2	4.8	43.80	19.73	52
	S-M3	6.45	41.20	18.08	51.64
	S-M4	4.14	45.52	21.12	53.1
	S-M5	5.38	42.30	19.05	55.2
	S-M6	7.18	43.30	23.25	51.5
	SA1	4.17	45.40	25.5	50.4
	SA2	4.43	41.72	18.4	48.7
	SA3	5.53	40.05	16.36	49.1
	SA4	4.51	42.32	22.7	52.1
	SA5	5.52	43.35	19.67	50.7
	SA6	5.26	40.50	22.84	53.12
	B1	6.06	47.80	31.34	26.81
	B2	10.86	46.30	35.4	36.74
	B3	6.21	43.90	34.11	26.85
	B4	5.27	44.90	30.23	28.87
	B5	9.59	45.80	31.23	27.76
	B6	7.63	47.20	33.23	30.69
	AG-E1	11.51	42.50	18.24	34.6
	AG-E2	12.72	40.70	16.4	33.9
	AG-E3	11.73	36.30	22.91	34.8
	AG-E4	9.97	38.60	19.93	37.7
	AG-E5	11.48	41.25	21.42	39.4
	AG-E6	12.66	40.50	18.6	40.1
Silty Loess	AG1	5.28	48.40	28.94	31
	AG2	5.7	51.80	36.65	30.7
	AG3	5.72	49.50	29.65	32.84
	AG4	6.68	50.70	29.45	33.2
	G-C1	7.2	49.60	41.13	32.6
	G-C2	7.71	46.50	33.38	32.7
	G-C3	7.77	47.80	40.1	34.2

Soil Type	sample Number	w %	n%	CaCO3%	LL%
Silty Loess	G-C4	8.31	48.60	38.9	35.5
	F1	4.73	39.45	20.4	29.5
	F2	4.03	38.40	21.2	24.3
	F3	4.65	39.52	28.7	31.2
	F4	4.38	38.90	22.54	27.42
	F5	4.75	39.70	23.15	33.05
	F6	4.9	38.73	23.35	35.1
	CH1	5.24	44.40	24.1	22.1
	CH2	7.16	40.20	26.2	22.4
	CH3	8.8	40.33	30.1	19.85
	CH4	8.53	42.30	28.65	24.11
	CH5	7.16	43.60	28.43	19.86
	CH6	6.42	41.12	27.54	17.65
Sandy Loess	AL1	4.47	46.40	35.41	-
	AL2	3.45	50.80	23.37	-
	AL3	5.46	42.10	36.65	-
	AL4	5.23	47.32	31.15	2.4
	AL5	4.91	49.68	32.52	5.3
	AL6	5.38	44.52	33.05	7.2
	T1	4.95	48.30	36.16	18.03
	T2	4.16	49.70	39.05	17.7
	T3	5.63	47.20	32.33	18.3
	T4	6.5	47.65	34.4	19.5
	T5	5.32	48.12	36.53	18.2
	T6	5.63	49.25	33.8	19.8
	H1	4.1	49.80	41.4	-
	H2	3.3	51.30	33.2	-
	H3	5.32	44.20	38.9	-
	H4	4.8	48.52	36.32	5.1
	H5	5.6	49.62	35.46	7.3
	H6	3.8	46.36	38.83	4.9

Tab. 1 - The physical and mechanical properties of Loess samples. W%: Natural water content, n%: Porosity, CaCO3%: Calcium carbonate, LL%: Liquid limit

Ultimately, the ROC curves were judged with the assistance of the predictive capability or the susceptibility maps' competence. It is a plot that sets the relationship between sensitivity against the specificity of the model at a series of thresholds for a positive outcome. The determination of the AUC enables the quantitative evaluation of the overall predictive capability of susceptibility models.

Data preparation

The loess cave inventory map is crucial for studying the loess cave talent and risk. Figure 3 presents the map of loess deposits distribution and the loess cave spreading in the study area.

In the present study, 697 loess caves have been recognized from Google earth images and numerous field surveys. The maximum and minimum diameters of the loess caves are 58.41 m and 0.34 m, respectively, whereas the maximum depth is 37.2 m and the minimum depth is 0.28 m. An investigation of 78 caves in the northern part of Cheshmehli village found that 89% of the loess caves were between 2 and 3.5 m wide. An investigation of 98 loess caves in the Hootan region of Golestan Province found the maximum width to be 3.8 m; however, the widths generally

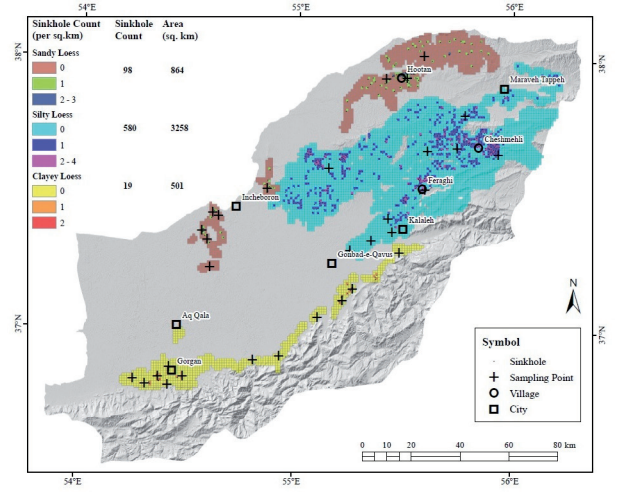

Fig. 3 - Distribution of loess deposits and spatial distribution of sinkholes (n=697) in loess zones of Golestan Province, projected on a map

ranged from 0.28 to 2.4 m. Investigations have shown that the height/width ratio for loess caves in Cheshmehli village is usually between 0.75 and 1.33; in the Hootan region, the ratio is 0.91-1.4; in the West of Province, the ratio is 0.76 -1.52: in Gonbad-Kaleleh, the ratio is 0.78-1.29: and in the central part of the study area is 0.64-1.24.

Loess cave conditioning factors

In susceptibility evaluation, it is crucial to select proper parameters for modeling because the selection factors in the training data set may be interdependent, leading to noise and errors in the model (Chen *et alii*, 2018). This study chose six loess cave conditional factors to demonstrate the areas at risk of loess caves. Figure 5 shows the joint density, land use, soil type, sensitivity collapse, self-weight collapse coefficient, and surface water distance maps.

Joint density

Loess joints, cracks, fissures, faults, bedding planes, and weak layers are geo-hazards, such as extensive erosion and effective land use. Loess caves associated with the loess joint, cracking–sliding failure, gully and landform fragmentation usually destroy houses, urban planning and construction industrial and agricultural, roads, sewers, flood-control dikes, channels, and other infrastructure (Xu *et alii*, 2016), and cause damage to the environment (Wang *et alii*, 2009). Earth fissures can develop due to ground-water withdrawal (e.g., Ghazifard *et alii*, 2016), horizontal tensile strain induced by local differential compaction (Bankher & Al-Harthi 1999), Freeze and thaw cycles (Li *et alii*, 2019), earthquakes (Vaz & Zezere 2016), active faults (Xu *et alii*, 2016), weak tensile characteristics of loess (Sun *et alii*,

Fig. 4 - Joints in loess plateau: a) The effect of tree roots on crack propagation (Sad Abad) b) Nearly parallel and equally spacing joint development (Seyyed Miran) c) Surface water accumulation and formation of mud cracks and joints (Alagol) d) Washing holes developed along the vertical joints, and vertical joints developed on the back scarp of the loess caves e) Ground cracking due to soil collapse (Ferraghi city).

2009), landslides (Wang *et alii*, 2010), underground mining (Li *et alii*, 2004), wetting-drying cycles (Xu *et alii*, 2017), biological processes (Richthofen, 1882), the combination of bending and shearing (Budhu, 2007) soil collapse (Li *et alii*, 2018), and changes in the physicochemical properties of soils (Ayalew *et alii*, 2004). Rainwater or surface water has collected in depressions or animal nests that infiltrated down along the loess joints and caused the loess to collapse. Eroded loess landforms refer to areas where Earth cracks are most common in the Golestan Province and the Gorgan Plain. They may be several meters long, several meters wide, and tens of meters deep. Combining ground-water withdrawal, earthquakes,

active faults, low tensile strengths of loess, biological processes, soil collapse, and aerial desiccation can produce joints in the Gorgan plain (Fig 4). Datasets needed to conduct hazard mapping of the earth joints include a comprehensive inventory of earth fissures, a digital geologic map, and a digital map showing the distribution of faults. These datasets are rasterized at 1000 m grid spacing using ArcGIS software.

Notably, from field surveys and loess cutting walls, the location of 8449 joints was recorded, and a map of their geographical distribution was prepared. The joint density map was categorized in four classes (Fig. 5a).

Land use

One of the parameters was land use, which plays a vital role in spreading loess caves' positions (Karminejad *et alii,* 2020). In addition, established on the land use map, in the rangeland, the occurrence of loess caves was denser than those in the agricultural land (Arabameri *et alii*, 2019). It shows the potential of rangeland (higher humidity than agricultural land) to variation to badland. In particular, we considered eight land use categories (Fig. 5b).

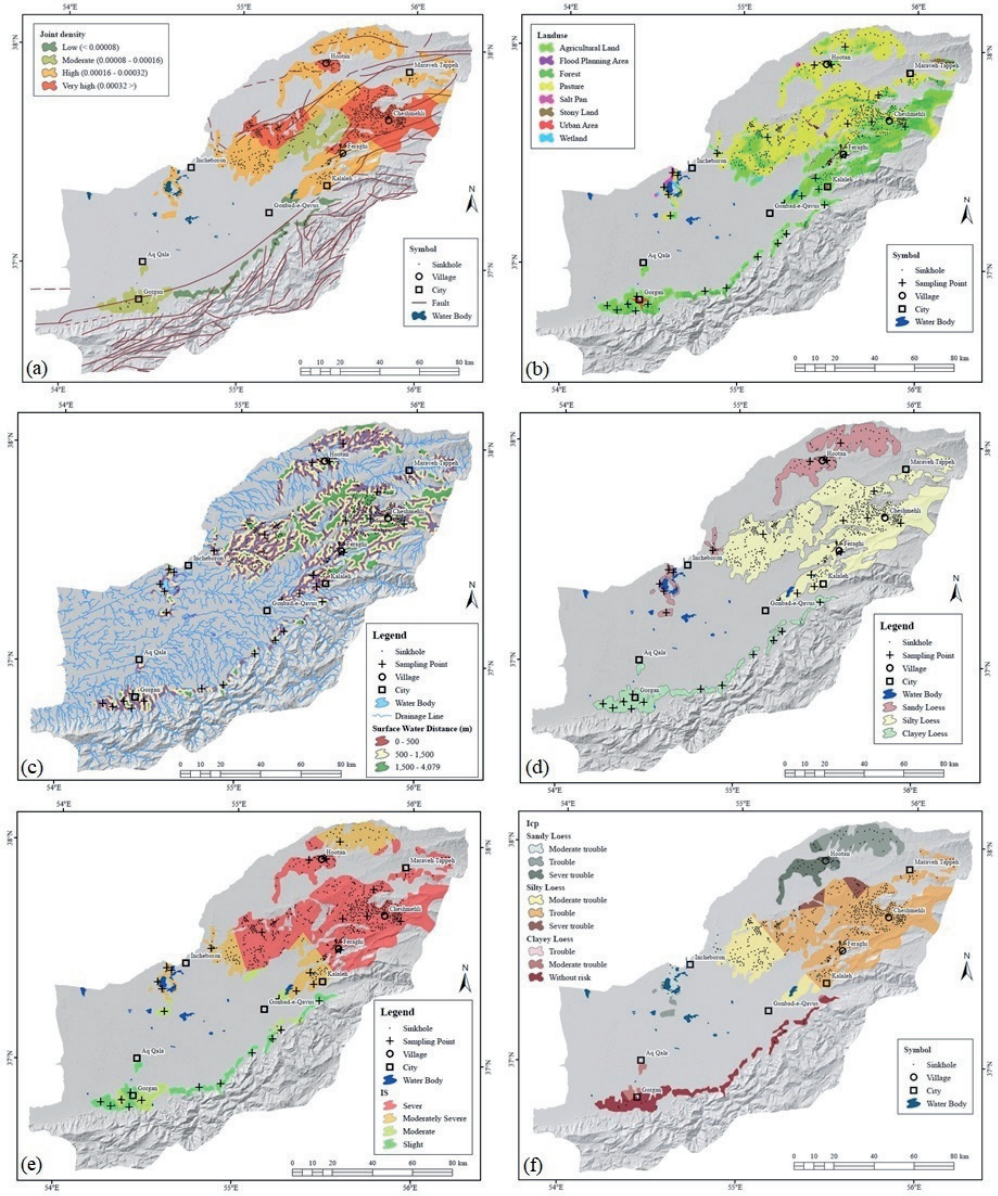

Fig. 5 - Maps of six causal factors in loess cave susceptibility: a) Classified joint density b) Classified land use c) Classified distance from surface water d) Classified loess type e) Classified collapse sensitivity f) Classified self-weight collapse coefficient

Surface water distance

The drainage density is one of the main factors that have a determining role in loess caves, as in some hillsides with low slopes, waterway and loess cave density are high (Fig.6). Rivers can cut and eroding riverbanks. This layer was prepared and digitized as practical factors in landslide occurrence (independent variables) in ArcGIS. We used the distance to rivers as the index to reflect the effect of rivers on loess caves, and the factor had three classes (Fig. 5c).

Collapse sensitivity

Some new research have revealed that although some areas have a higher collapse coefficient (Ic), the hazard of damaging phenomena in these areas may be lower than those with a lower Ic (Cui, 2010). The idea of collapse sensitivity (Is) is well-defined based on the magnitude and speed of collapse (Zhang *et alii*, 2018). In the current study, by leading laboratory experiments on loess soils of Golestan Province, the values of Ic and collapse speed of soil (T90%) were calculated,

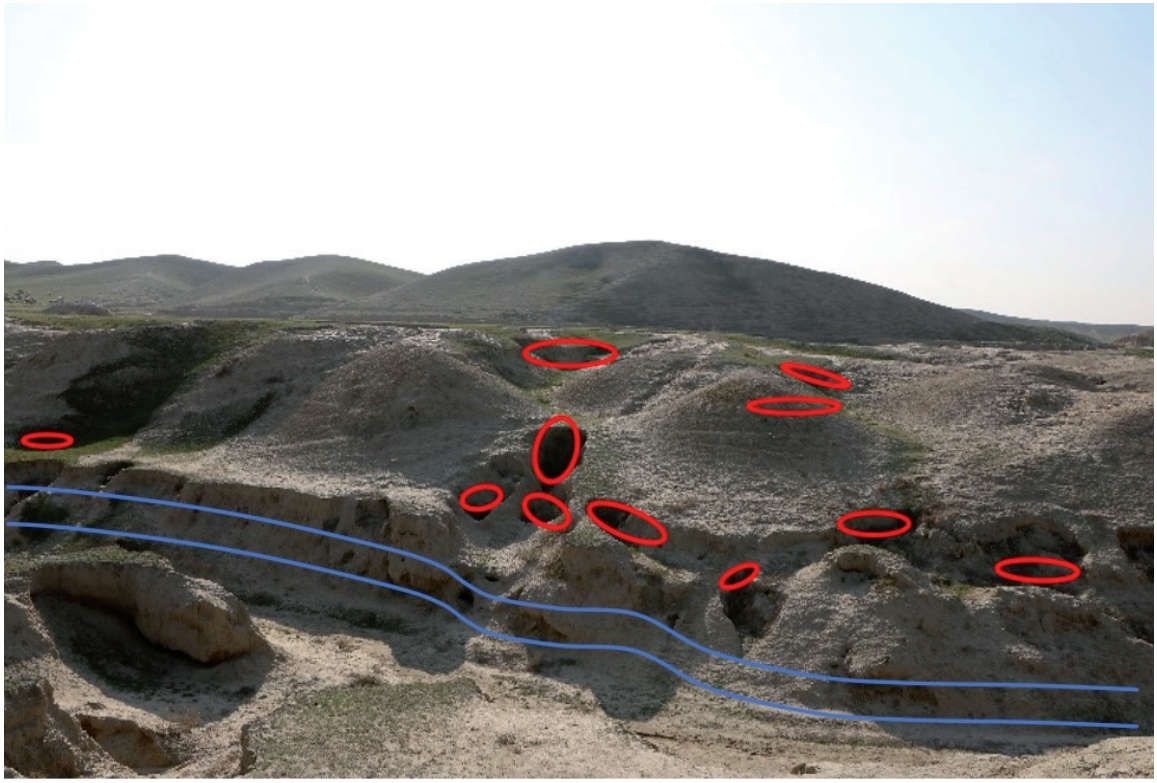

Fig. 6 - Development of loess caves around the seasonal river (Maraveh Tappeh)

Soil-type

Soil-type conditions of the study area are very vital in cave occurrence. From a lithological viewpoint, the vulnerable region to cave occurrence in Golestan Province is where the soils cover silty and sandy loess. Soil properties control the occurrence and development of caves (Bernatek-Jakiel *et alii* 2016). These properties were attained from the laboratory tests of 60 undisturbed block samples gathered in the vicinity of the loess cave. Based on the geotechnical and sedimentological characteristics of the loess soils of the study area, from south to north, these features are divided into clayey (Zone I), silty (Zone II), and sandy loess soils (Zone III), respectively (Rezaiy *et alii*, 2011). This factor is divided into three class maps (Fig. 5d).

and the grade of collapse sensitivity was determined. T90% can be calculated from the laboratory data (ASTM D5333-03 2003). Since the two parameters of collapse magnitude (Ic) and collapse speed (T90%), the criterion of soil collapse sensitivity is shown in Table 2. Using the outcomes of laboratory tests, we separated the soils into four classes based on the value of the Ic: Ic <1.5, 1.5 < Ic ≤3, 3 < Ic ≤ 7, Ic > 7.

In addition, soils are separated into four groups based on T90%: T90% < 5 min, 5 < T90% ≤ 15min, 15min < T90% ≤ 60 min, T90% > 60 min.

Based on two causes, magnitude (Ic) and time of collapse (T90%), soils are separated into four classes with collapse sensitivity (Is) low, medium, medium to severe, and severe. We calculated Ic and T90% values for 60 points in Golestan

T (min)	$I_{c.}$ (%)		
	$0.015< I_C \leq 0.03$	$0.03< I_C \leq 0.07$	$I_C > 0.07$
$60 < T$	Slight	Slight	Moderate
$15 < T \leq 60$	Slight	Moderate	Moderate severe
$5 \leq T \leq 15$	Moderate	Moderate severe	Severe
$T < 5$	Moderate severe	Severe	Severe

Tab. 2 - Grades of collapse sensitivity in loess (Zhang et alii, 2018)

Soil Type	sample Number	ICp	IS
clay Loess	S-M1	0.14	Slight
	S-M2	0.31	Moderate
	S-M3	0.22	Slight
	S-M4	0.34	Slight
	S-M5	0.45	Slight
	S-M6	0.58	Slight
	SA1	0.53	Slight
	SA2	1.12	Moderate
	SA3	0.67	Slight
	SA4	0.79	Slight
	SA5	0.54	Slight
	SA6	0.66	Slight
	B1	0.88	Slight
	B2	0.24	Slight
	B3	0.27	Moderate
	B4	0.15	Slight
	B5	0.19	Slight
	B6	0.84	Slight
	AG-E1	0.11	Slight
	AG-E2	0.08	Slight
	AG-E3	0.06	Slight
	AG-E4	0.04	Slight
	AG-E5	0.07	Slight
	AG-E6	0.07	Slight
Silty Loess	AG1	1.54	Moderate
	AG2	1.67	Moderately severe
	AG3	3.25	Moderately severe
	AG4	4.2	Moderate
	G-C1	1.52	Moderately severe
	G-C2	2.2	Moderately severe
	G-C3	1.78	Moderately severe
	G-C4	2.56	Moderate
Silty Loess	F1	5.4	Sever
	F2	5.12	Sever
	F3	6.17	Sever
	F4	5.19	Sever
	F5	6.34	Sever
	F6	6.95	Sever
	CH1	6.58	Sever
	CH2	7.44	Sever
	CH3	8.4	Sever
	CH4	7.68	Sever
	CH5	6.95	Sever
	CH6	8.24	Sever
Sandy Loess	AL1	6.58	Moderately severe
	AL2	8.14	Moderately severe
	AL3	6.56	Moderately severe
	AL4	7.14	Moderately
	AL5	7.19	Moderately severe
	AL6	8.16	Moderately
	T1	1.5	Moderate
	T2	1.63	Moderately severe
	T3	1.87	Moderately severe
	T4	3.32	Moderate
	T5	4.89	Moderately severe
	T6	5.4	Moderately severe
	H1	8.64	Sever
	H2	7.77	Moderately severe
	H3	11.57	Sever
	H4	12.25	Moderately severe
	H5	8.84	severe
	H6	7.19	Moderately severe

Tab. 3 - Grades of collapse sensitivity of loess soils and variation of ICp in Golestan Province

Province, and the collapse sensitivity condition of loess soils in three Zones I, II, and III were determined (Table 3). This layer is separated into four groups (Fig. 5e).

Self-weight collapse coefficient

Loess deposit has distinct collapse specifications. Collapsible loess has been responsible for severe soil and water loss and has been known to aggravate and even induce the development

Fig. 7 - Crack initiation in loess soils due to self-weight collapse (Cheshmehli village)

of loess caves, mudslides, and landslides (Bernatek-Jakiel & Poesen 2018; Li L *et alii,* 2017). Loess collapse is mainly caused by the destruction of large and medium pores, although the contribution of the middle pores on the collapse. The changes in the physical state and strength of the loess occur mainly under the action of inundation. The particle connections are destroyed, fine particles fall into the large pores, and deformation rapidly increases. After the loess collapses, there is larger-scale destruction of the loess layer structure, and this causes whole-scale ground subsidence or collapse and forms a collapsible crack around the subsidence area (Fig.7).

In general, if the wetting direction occurs from the top loess layer to the bottom loess layer, the occurrence of collapse deformation is also gradually carried out from the top layer to the bottom layer of the loess, and this is beneficial to the formation of loess caves or plate-shaped depressions (Fig.8).

The developmental regionalization of loess caves and the self-weight collapsibility are closely related. The loess caves are often developed in the zones where the loess collapsibility is intense, especially the zones where the self-weight significantly contributes to the collapse process, such as Hootan-Korand in zone III and Cheshmehli and Feraghi in zone II. The self-weight collapsibility (Icp) here is more than200 times that of others (Table 3). Therefore, we can conclude that the loess collapsibility, especially the self-weight collapsibility is a primary internal cause that influences the development of loess caves. It was divided into four classes (Fig. 5f).

BIVARIATE STATISTICAL METHOD

Each loess cave casual factor map is combined with the loess cave inventory map in the bivariate statistical method. The occurrence of loess cave is supposed to be a dependent parameter, and another environmental variable is regarded as an independent variable. The weights are derived from either loess cave abundance or densities in each attribute class within each factor. Under the probability principle, spatial densities correlate with

Fig. 8 - The formation of a) plate-shaped depressions and b) loess caves

the chosen casual factors classes' susceptibility to the destructive operation liable for developing the considered loess cave. Some casual factors included soil type, self-weight collapsibility, land use, river distance, joint density, and sensitivity collapse maps to classify the loess cave susceptibility zones. Lastly, we generated a map of loess cave susceptibility mapping through the algebraic addition of the Information Value maps of parameters and the previously obtained classifications. Mainly three weight estimation methods have been employed in the bivariate statistical method: Information Value method, Frequency Ratio, and Density Area. After comparing determining factors and creating weight maps, the best and the most exact method can be presented. Later, these methods will be given in detail.

Information Value (IF) method

In the Information Value model, the weighted class value is calculated through the density of loess caves regarding each determining factor. For spatial landslide zonation, the Information Value model has been employed by many researchers such as; Mengistu *et alii* (2019), Balasubramani, and Kumaraswamy (2013). The Information Values of numerous determining factors can be used to detect the potential areas of loess cave occurrence, which may simplify loess cave hazard zonation. The Information Values can be determined based on the appearance or nonappearance of the determining factor classes within the past loess cave. The loess cave map can be combined with the determining factor maps to calculate the weights for relevant classes. Thus, the overlay makes the loess cave hazard zonation (CHZ.) map of the loess cave map with different factor maps. If the Information Value is positive, the determining factor class represents a strong relationship with the loess cave in the area. The weighted value of a causative factor class can be represented as the natural logarithm of density of loess cave in a factor class, divided by loess cave density in the total map area.

The Information Value can be computed by utilizing eqs. 1 and 2(Yin & Yan, 1988);

$$Wi = \ln\left(\frac{Densclass}{Densmap}\right) = \ln \frac{Npix(S_i)/Npix(N_i)}{\sum_{i=1}^{n} Npix(S_i) \Big/ \sum_{i=1}^{n} Npix(N_i)} \qquad (1)$$

where *Wi* is the weight given to the class of a specific thematic layer (e.g., sandy loess in the thematic layer soil type), *Densclass* is the loess cave density within the thematic class, *Densmap* is the loess cave density within the total thematic layer, *Npix(Si)* is the number of loess cave pixels in a specific thematic class, *Npix(Ni)* is the total number of pixels in a specific thematic class, and n is the number of classes in a thematic map. The natural logarithm is used to accommodate the considerable variation in the weights. The weight map of the determining factors can be overlayed and combined in a GIS environment; each thematic layer's total weight (*Wi)* in the study area is detected and illustrated in Table 3. To conclude, the outcoming weighted layers were summed up (Eq. 2) to make a loess cave Susceptibility Index (CSI) map:

$$W_{ij} = W_{iJointdensity} + W_{iLanduse} + W_{iSurfacewaterdistance} + W_{iSelfweightcollapsecoefficient} + W_{iSoiltype} + W_{iSensitivity} \qquad (2)$$

where, $W_{iJointdensity}$, $W_{iLanduse}$, $W_{iSurfacewaterdistance}$, $W_{iSelfweightcollapsecoefficient}$, $W_{iSoiltype}$, $W_{iSensitivity}$ are distribution-derived weights of the joint density, land use, surface water distance, self-weight collapse coefficient, soil type, and collapse sensitivity, respectively.

DENSITY AREA (DA) METHOD

In this model, similar to the Info Val model, the loess cave density for each factor map is computed using Eqs. 3 and 4, the

CHZ map is generated the same as the Info Val method (Lee & Kyungduck, 2001).

$$D_{area} = \frac{Npix(SXi)}{Npix(Xi)} \quad (3)$$

$$W_{area} = 1000\left[D_{area} - \frac{\sum Npix(SX_i)}{\sum Npix(X_i)}\right] \quad (4)$$

Darea is the loess cave density in each hazard class, *Warea* is the area density index, *Npix (SXi)* is the area of happened loess cave in each class or variable *Xi*, *Npix (Xi)* is the area of each class or variable *Xi*. The best equation for causative factors and loess cave absence and presence as well as loess cave susceptibility map was produced in software Arc GIS., then classified based on turning points of cumulative frequency curves of pixels in five classes of susceptibility, including very high, high, medium, low, and very low.

FREQUENCY RATIO (FR) METHOD

The Frequency Ratio model gives each input layer the proportion of loess cave cells in the specific category. It can be described as the ratio of the relative frequency of loess cave cells in a category (an attribute class) to the relative frequency of all loess cave cells in the area. This model includes more independent variables that play a significant role in determining the dependent variables. One of the serial comprehensive linear models is beneficial for analyzing dependent variables and anticipating loess cave instability. The Frequency Ratio can be expressed as follows:

$$Fr_i = \frac{Npix(S_i)/Npix(N_i)}{\sum Npix(S_i)/\sum Npix(N_i)} \quad (5)$$

where, *(Si)* is the number of loess cave cells in category *i*, *(Ni)* is the total number of cells in category *i*, *Σ(Si)* is the total number of landslide cells loess cave, and *Σ(Ni)* is the total number of cells. To calculate the loess cave susceptibility index (CSI), each factor's Frequency Ratio values were summed to the training area as Eq. 6.

$$CSI = Fr1 + Fr2 + Fr3 + ... + Frn \quad (6)$$

This Frequency Ratio is normalized to '1'. If the value is higher than one, it shows a higher density of loess cave cells in the category than overall in the dataset. It means a higher correlation. If the value is lower than 1, it indicates a lower correlation. Results lower than 1 point to categories with a density of loess cave cells lower than the density in the dataset. Among the bivariate statistical approaches, Frequency analysis is the most commonly used method (Chimidi *et alii*, 2017). The related factors with loess cave occurrence were prepared (Table 4).

The overlay analysis will thus provide a ratio between loess cave that 'did' occur to the loess cave that 'did not occur within each causative factor loess cave class, and the area ratio to the entire area was calculated.

Factor	Class	Area (pix)	Loess caves Area (pix)	InfoVal weight (ln)	Density area weight	Frequency ratio weight
Soil Type	Sandy Loess	960091	98	-0.284686299	-0.033617443	0.752250199
	Silty Loess	3619989	580	0.166176131	0.02453038	1.180781056
Joint Density	Low	283563	11	-1.252124651	-0.096893574	0.28589672
	Moderate	738918	36	-1.024253619	-0.086965774	0.359064364
	High	2561277	233	-0.399808391	-0.044715413	0.670448498
Self-weight Coefficient	Without risk	496110	19	-1.2649443	-0.097387701	0.282255017
	Moderate trouble	967956	122	-0.07375119	-0.009646872	0.928902785
	Trouble	3249822	508	0.14154034	0.020630594	1.152046977
Land use	Agricultural Land	1772940	214	-0.117044156	-0.014987637	0.889545914
	Forest	557082	45	-0.518675663	-0.054913047	0.595308415
	Pasture	2636187	407	0.129098645	0.018698554	1.137802357
	Urban Area	44882	2	-1.113515349	-0.091129807	0.32840248
	Stony Land	42236	9	0.451325933	0.07739726	1.570393042
Surface Water Distance	0-500	2051983	332	0.175947341	0.026103612	1.192375268
	500-1500	2300331	291	-0.070110744	-0.009187567	0.932290569
Collapse Sensitivity	Sever	3368379	590	0.252022445	0.039020519	1.286624915
	Moderately Sever	1093033	88	-0.525288059	-0.055627997	0.591384986
	Moderate	304117	14	-1.08426836	-0.090103003	0.338149099

Tab. 4 - Computed weights for classes of various thematic data layers based on loess cave occurrences using the bivariate statistical methods

RESULTS AND DISCUSSION

Because loess cave occurrences are the products of synchronous impacts of intrinsic and environmental factors in each map unit and the existence of a correlation between these influencing factors, the entire risk of loess cave occurrence would be similar to the happening probability of all the influencing factors. Therefore, the ultimate weight of each pixel would be equal to the algebraic sum of all influencing factors, weight in that unit. This objective is attained by overlaying and combining weight influencing factor maps. Subsequently, after counting the weight of different effective influencing factor layers of loess cave, and from overlaying these influencing layers, and employing the bivariate statistical methods in this research, a final loess cave hazard map was generated. Loess cave susceptibility maps for four models are shown in Figures 9 to 11.

The prepared Loess cave susceptibility maps of the Golestan Province were classified into five zones, i.e., very low, low, moderate, high, and very high susceptibility (Table 5 and Figs. 9 to 11).

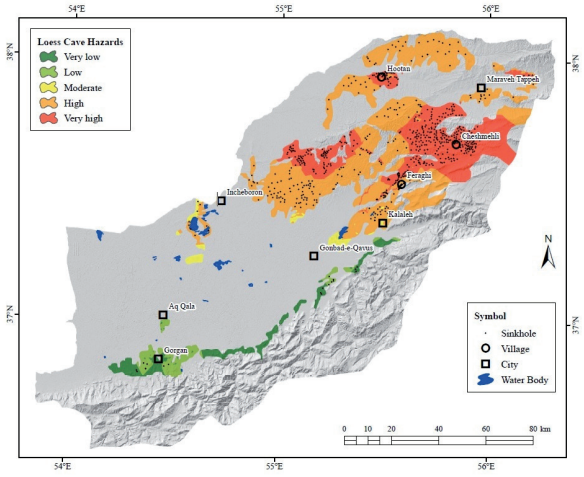

Fig. 9 - Final loess cave hazard zonation map produced by the Information Value method

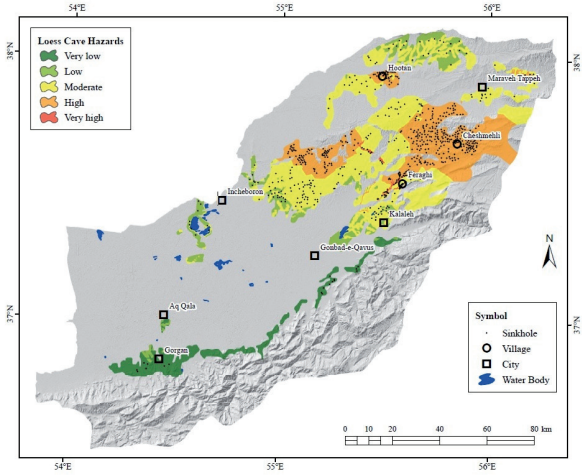

Fig. 10 - Final loess cave hazard zonation map produced by the Frequency Ratio method

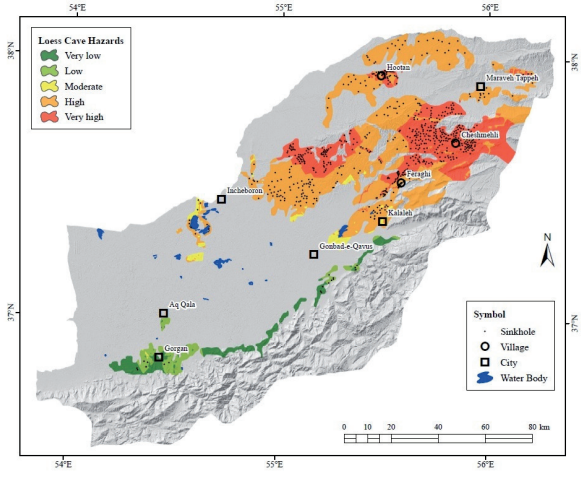

Fig. 11 - Final loess cave hazard zonation map produced by the Density Area method

These methods were applied to ensure the relationship between the influencing factors, and 697 the loess caves results are shown in Table 4. As for the (Is) factor, 84.64 % of loess caves for severing sub-class and moderate-severe sub-class were 12.6%, respectively, meaning that 97.24% of loess caves were distributed among the two sub-classes of Is factor. For the land-use factor, 51.32 % of loess caves for the pasture subclass and agriculture subclass were 34.51%, respectively, meaning that 85.83 % of loess caves were distributed between the two sub-classes of the land-use factor. Besides, for the soil type factor, 70.47% of loess caves for the silty loess sub-class and sandy loess sub-class were 18.69%, respectively, which means that 89.16% of loess caves were distributed between the two classes of soil type. For the joint density factor, 49.86% of loess caves for the high subclass and very high subclass were 30.23%, respectively. In addition, for the surface water distance factor, 44.78 % of loess caves for (500-1500 m) sub-class and for <500m sub-class were 39.94 %, respectively.

In all methods at collapse sensitivity factor, the sever subclass; among soil type, silty loess subclass, land-use factor, flood plain area subclass, and self-weight collapse factor, the trouble subclass have the highest weights. In addition, land use factors have the highest weight in all methods. In addition, according to the results (Table 4), all factors in the FR method are higher than others.

The result of the IF model showed that the study area was dominated by a high loess cave susceptibility zone (57.69%) and followed by a very high loess cave susceptibility zone (28.92%), very low, low, and moderate loess cave susceptibility zones respectively. The application of DA and FR models showed that in high, very high, and moderate loess cave susceptibility zones, 30.57%, 0.37 %, and 47.82 % pixels are being affected by loess caves, respectively. The results with the IF model (86.61%) indicated that a considerable part of the study area was located in high to very high hazard classes. However, the results of DA and FR models (78.76%) show that 78.76 % of the study area was located in moderate, high to very high hazard classes. The bivariate methods were applied to explore the relationship between the occurrence of loess caves and the determining factors in this study, the results of which were essentially reliable in predicting the significant intervals of each factor.

PERFORMANCE AND COMPARISON OF DIFFERENT MODELS

Each model has its strengths and weaknesses, and commonly its performance varies with different study areas. Thus, it is suggested to compare various models to choose the most appropriate one. The Density ratio (*Dr*) index (Guzzetti *et alii*, 2000) is used to compare hazard classes in individual maps independently, which can be accounted for through Eq. 7 (Gee, 1992).

$$Dr = \frac{\frac{S_i}{A_i}}{\frac{\sum_i^n S_i}{\sum_i^n A_i}} \quad (7)$$

where, *Dr* is loess caves density in each hazard class, Si is the total number of loess caves in each hazard class, *Ai* is the area for each hazard class in the zonation map, and n is the number of a hazard class. In a zonation method, loess cave density in a hazard class with *Dr* = 1, i.e., having a density equal to the average loess cave density of all the region, and a class density ratio of 2, has a loess cave density equal to two times of the loess cave density of the area. The density ratio (*Dr*) for the IF method in the hazard class is very high, accounting for 2.038. The amounts are the same for DA and FA models and equal to 3.817 (Table 5).

Method	Hazard Classes	Ai	Si	D.R.
InfoVal weight (ln)	Very Low	324506	6	0.135811837
	Low	229727	13	0.41566209
	Moderate	130804	2	0.112309909
	High	2953965	265	0.658945709
	Very High	1480667	411	2.038888753
		5119669	697	
Density area weight	Very Low	524160	19	0.266255649
	Low	562411	38	0.496293853
	Moderate	2448605	213	0.638954565
	High	1565250	417	1.956867624
	Very High	19243	10	3.817124504
		5119669	697	
Frequency ratio weight	Very Low	524160	19	0.266255649
	Low	562411	38	0.496293853
	Moderate	2448605	213	0.638954565
	High	1565250	417	1.956867624
	Very High	19243	10	3.817124504
		5119669	697	

Tab. 5 - Accounted values for density ratio

Loess cave susceptibility maps can be verified by comparing the susceptibility maps with the training data used for building the models with the validation data that were not used during the model building process. The compatibility of the susceptibility models was evaluated using the training dataset. Correspondingly, their prediction probability was assessed using the validating dataset. The susceptibility maps' predictive capability or competence was judged using the ROC curves (Zizioli *et alii*, 2013). It is a plot that sets the relationship between sensitivity (proportion of true positives) against specificity (proportion of false positives) of the model at a series of thresholds for a positive outcome. The sensitivity, which is plotted on the y-axis, is the likelihood that the area with a loess cave is correctly classified, while specificity (false negative rate) is the probability that the area with the no-loess cave is correctly classified. The x-axis expressed as 1 - specificity represents the false positive rate (Jaiswal *et alii*, 2010). The determination of the AUC enables the quantitative evaluation of the overall predictive capability of the susceptibility model (Beguería, 2006), ranging between 0 and 1. A value closer to 1 indicates the good predictive ability of the model. A casual predictive power will be manifested for an AUC value of about 0.5, describing a diagonal straight line. AUC value below 0.5 means models with a terrible predictive capacity and should not be taken into consideration. The mathematical expression of the AUC is given by Equation 8 (Pereira *et alii*, 2012).

$$AUC = \sum_{i=1}^{n} \left[\left(x_{i+1} - x_i \right) \times \frac{y_{i+1} + y_i}{2} \right] \quad (8)$$

where *x* is the portion of the study area predicted as susceptible by descending order and *y* is the percentage of correctly classified loess cave area belonging to the validation group. AUC values between 0.70 and 0.80 correspond to an acceptable model, while AUC values ranging between 0.8 and 0.9 indicate an excellent susceptibility model, and finally, AUC values > 0.9 typify excellent models. The area under the curve approach was used, and the results are shown in Table 6 and Figure 12.

				Asymptotic 95%	Confidence interval
Test result variable(s)	area	Std. Error[a]	Asymptotic Sig.[b]	Lower Bound	Upper Bound
Frequency	0.702	0.011	0.000	0.680	0.725
Density	0.702	0.011	0.000	0.680	0.725
Infoval	0.702	0.011	0.000	0.682	0.727

Tab. 6 - The test result variable (s): Frequency, Density, Infoval has at least on tie between the positive actual state group and the negative actual state group. Statistics may be biased.
a. Under the nonparametric assumption
b. Null hypothesis: true area=0.5

The AUC of the IF model was 0.727. The values of AUC for DR and the FR models were similar and equal to 0.725. Respective AUC values for all models showed that the map obtained from the models accurately classified the areas of existing loess caves. For the prediction capacity evaluation of the developed loess cave models, the prediction rate curve was obtained using the loess cave pixels in the validating dataset (30% of the total observed loess caves). It can be seen from Figure 6 that three models have a good prediction capability (AUC ≥ 0.727), and the prediction capacities of the three models can be evaluated relatively similarly.

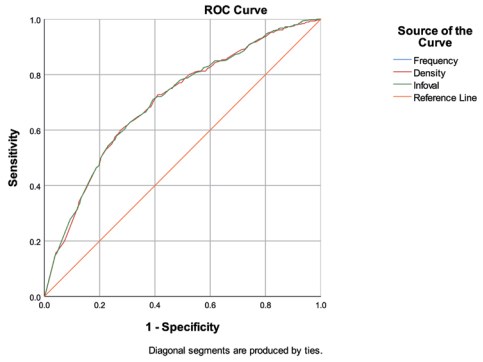

Fig. 12 - ROC curve of the models

CONCLUSIONS

Preparing the loess cave susceptibility map was a vital step forward in Golestan Province's hazard mitigation. In the current study, three models based on bivariate methods as FR, DA, and IF were used to zoning loess cave hazard, and their efficiency and performance are compared in Golestan Province, NE Iran, and the following conclusions can be drawn:

- the FR and DA models performed the best in terms of accuracy, and the loess cave susceptibility map constructed by these models was appropriate and analytical. The amounts of density ratio show that DA, IF and FR methods have good accuracy and applicability within all the three used methods to separate hazard classes by the density ratio index in the studied area;

-through FR, IF, and DA methods, land use, joint density, and sensitivity collapse factors impact loess cave occurrence;

-the calculated results of the ROC curves show that in the used models in this study, all methods are the accepted model for the studied area;

- the results from all models show that collapse sensitivity (Is) is the most critical factor affecting loess caves occurrence. So, 84.64 % of loess caves are distributed in the severe subclass for Is influencing factor;

- in the all model, agricultural lands and pastures land-use factors were essential in loess cave occurrence;

- to determine the exact extent of loess cave destruction, areas within high and very high loess cave susceptibility categories require more site detailed studies by engineering geologists before commencing development.

ACKNOWLEDGMENTS

The Engineering Geology and Geotechnics laboratory of Bu-Ali Sina University is appreciated for providing the laboratory tests. The comments of anonymous reviewers were very helpful in improving the manuscript.

REFERENCES

Amiri M., Pourghasemi H. R., Ghanbarian G. A., Afzali S. F. (2019) - *Assessment of the importance of gully erosion effective factors using Boruta algorithm and its spatial modeling and mapping using three machine-learning algorithms*. Geoderma, **340**: 55-69. https://doi.org/10.1016/J.GEODERMA.2018.12.042

Arabameri A., Pradhan B., Rezaei K., Sohrabi M., Kalantari Z. (2019) - *GIS-based landslide susceptibility mapping using numerical risk factor bivariate model and its ensemble with linear multivariate regression and boosted regression tree algorithms*. Journal of Mountain Science, **16**(3): 595–618. Doi: 10.1007/s11629-018-5168-y

ASTM International (2003) - ASTM D5333-03. *Standard test method for measurement of collapse potential of soils*. ASTM International, West Conshohocken, PA.

Bai S., Wang J., Lu G., Zhou P., Hou S., Xu S. (2010) - *GIS-based logistic regression for landslide susceptibility mapping of the Zhongxian segment in China's Three Gorges area.* Geomorphology, **115**: 23–3.

Balsubramani K. & Kumaraswamy K. (2013) - *Application of geospatial technology and information value technique in landslide hazard zonation mapping: a case study of Giri Valley, Himachal Pradesh*. Disaster Adv, **6**: 38–47.

Bankher K. A. & Al-Harthi A. A. (1999) - *Earth fissuring and land subsidence in Western Saudi Arabia*. Natural Hazards, **20**(1): 21–42.

Beguería S. (2006) - *Validation and Evaluation of Predictive Models in Hazard Assessment and Risk Management*. Natural Hazards, **37**(3): 315-329.

Bernatek-Jakiel A., Kacprzak A., Stolarczyk M. (2016) - *Impact of soil characteristics on piping activity in a mountainous area under a temperate climate (Bieszczady Mts., Eastern Carpathians).* CATENA, **141**: 117–129.

Bernatek-Jakiel A. & Poesen J. (2018) - *Subsurface erosion by soil piping: significance and research needs.* Earth-Sci. Rev., **185**(1): 1107-1128.

Budhu M. (2007) - *Soil Mechanics and Foundations*. John Wiley & Sons, New York. 761 pp.

Chen W., Xie X., Peng J., Shahabi H., Hong H., Bui D. T., Duan Z., Li S. & Zhu A. (2018) - *Gis-based Landslide Susceptibility Evaluation Using a Novel Hybrid Integration Approach of Bivariate Statistical Based Random forest Method*. CATENA, **164**: 135–149. Doi:10.1016/j.catena.2018.01.012

Chen J., Shaw S. L., Yu H., Lu F., Chai Y. & Jia Q. (2011) - *Exploratory data analysis of activity diary data: a space-time GIS approach.* Journal of Transport Geography, **19**(3): 394–404. Doi:10.1016/j.jtrangeo.2010.11.00

Chimidi G., Raghuvanshi T. K., Suryabhagavan K. V. (2017) - *Landslide hazard evaluation and zonation in and around Gimbi town, western Ethiopia a*

GIS-based statistical approach. Applied Geomatics, **9**(4): 219–236.

Cui Y.E. (2010) - *Discussion on the issue of sensitivity of loess collapse*. Coal Eng., **8**: 76–78 (in Chinese). https://doi.org/10.3969/j.issn.1671-0959.2010.08.030.

De Martonne E. (1926) - *Aerisme, et índices d'aridite.* Comptesrendus de L'Academie des Sciences, **182**: 1395–1398.

Eftekharnejad J. & Behroozi A. (1991) - *Geodynamic significance of recent discoveries of ophiolites and late Paleozoic rocks in NE Iran (including Kope Dagh).* Abhandlungen der Geologischen Bundesanstalt, **38**: 89–100.

Feiznia S., Ghauomian J. & Khajeh M. (2005) - *The study of the effect of physical, chemical and climate factors on surface erosion sediment yield of loess soils (Case study in Golestan Province).* Pajouhesh-va-Sazandegi - Spring, **17**(1): 14-24.

Fletcher J. E. & Carroll P. H. (1949) - *Some properties of soils that are subject to piping in southern Arizona.* Soil Science Society of American Journal, **13**: 545–547.

Fuller M.L. (1922) - *Some unusual erosion features in the Loess of China.* Geographical Review, **12**(4): 570–584. https://doi.org/10.2307/208591.

Gee M. D. (1992) - *Classification of landslide hazard zonation methods and a test of predictive capability*. In: Proceedings 6th International Symposium on Landslides, Christchurch, New Zealand, **2**: 947–952.

Ghazifard A., Moslehi A., Safaei H., Roostaei M. (2016) - *Effects of ground-water withdrawal on land subsidence in Kashan Plain, Iran.* Bull. Eng. Geol. Environ., **75**: 1157–1168.

Ghorbanzadeh O., Meena S. R., Abadi H. S. S, Piralilou S. T., Zhiyong L., Blaschke T. (2021) - *Landslide mapping using two main deep-learning convolution neural network (CNN) Streams combined by the Dempster–Shafer (D.S.) model.* IEEE J. Sel. Top. Appl. Earth Obs. Remote Sensing. **14**: 452–463.

Ghobadi M. H., Nouri M., Saedi B., Jalali S. H. & Pirouzinajad N. (2017) - *The performance evaluation of Information Value, Density Area, LNRF, and Frequency Ratio methods for landslide zonation at Miandarband area, Kermanshah Province, Iran.* Arabian Journal of Geosciences, **10**(19). Doi: 10.1007/s12517-017-3202-y

Guzzetti F., Cardinali M., Reichenbach P. & Carrara A. (2000) - *Comparing landslide maps: a case study in the upper Tiber River Basin, Central Italy.* Environmental Managment, **25**(3): 247–363.

Hadmoko D. S., Lavigne F., Samodra G. (2017) - *Application of a semiquantitative and GIS-based statistical model to landslide susceptibility zonation in Kayangan Catchment, Java, Indonesia.* Natural Hazards, **87**(1): 437–468.

Halliday W. R. (2007) - *Pseudokarst in the 21st century.* Journal of Cave and Karst Studies, **69**: 103-113.

Hill C. & Forti P. (1997) - *Cave Minerals of the World*. 2nd ed., National Speleological Society Inc., Huntsville, U.S.A., 463 pp.

Jaiswal P., Van Westen C. J. & Jetten V. (2010) - *Quantitative Landslide Hazard Assessment Along a Transportation Corridor in Southern India*. Engineering Geology, **116**(3-4): 236-250. https://doi.org/10.1016/j.enggeo.2010.09.005.

Kariminejad N., Rossi M., Hosseinalizadeh M., Pourghasemi H. R. & Santosh M. (2020) - *Gully head modelling in Iranian Loess Plateau under different scenarios.* CATENA, **194**, 104769. Doi:10.1016/j.catena.2020.104769

Karimi A., Khademi H., Kehl M. & Jalalian A. (2009) - *Distribution, lithology and provenance of peridesert loess deposits in northeastern Iran.* Geoderma, **148**: 241–250

Keshavarzi B. (2014) - *A possible link between mineralogy of loess deposits and high incidence rate of esophageal cancer in Golestan province of Iran. Iranian J*ournal of Science and Technology (Sciences), **38**(3): 281-287. Doi: 10.22099/ijsts.2014.2273

Lara M. & Sepulveda S. A. (2010) - *Landslide susceptibility and hazard assessment in San Ramón Ravine, Santiago de Chile, from an engineering geological approach*. Environmental Earth Sciences, **60**: 1227–1243.

Lavrusevich A. (2019) - *Classification of the types and forms of loess pseudokarst.* E3S Web of Conferences, 135, 01041. Doi:10.1051/e3sconf/201913501041

Lee S. & Kyungduck M. (2001) - *Statistical analysis of landslide susceptibility at Yonging, Korea.* Environmental Geology, **40**:1095–1113.

Lee S. & Sambath T (2006) - *Landslide susceptibility mapping in the Damrei Romel area, Cambodia using Frequency Ratio and logistic regression models*. Environmental Geolology, **50**: 847–856.

Lee S. & Talib J.A. (2005) - *Probabilistic landslide susceptibility and factor effect analysis.* Environmental Geology, **47**(7): 982–990. Doi: 10.1007/s00254-005-1228-z

Li J., Wang F., Yi F., Wu F., Liu J. & Lin Z. (2019) - *Effect of Freeze-Thaw Cycles on Triaxial Strength Property Damage to Cement Improved Aeolian Sand (CIAS).* Materials, **12**(17), 2801.

Li L., Lan H., Guo C., Zhang Y., Li Q. & Wu Y. (2017) - *A modified Frequency Ratio method for landslide susceptibility assessment.* Landslides, **14**(2):727–741.

Li X., Wang S.J., Liu T.Y. & Ma F. S. (2004) - *Engineering geology, ground surface movement and fissures induced by underground mining in the Jinchuan Nickel Mine.* Engineering Geology, **76**(1-2): 93–107.

Mengistu F., Suryabhagavan K. V., Raghuvanshi T. K. & Lewi E. (2019) - *Landslide Hazard zonation and slope instability assessment using optical and*

InSAR data: a case study from Gidole town and its surrounding areas, southern Ethiopia. Remote Sensing of Land, **3**(1):1–14.

Peng J., Sunc P., Igwed O., Li X. (2017) - *Loess caves, a special kind of geo-hazard on loess plateau, northwestern China*. Engineering Geology, **236**: 79-88. Doi: 10.1016/j.enggeo.2017.08.012.

Pires L.F., Cooper M., Cássaro F.A.M, Reichardt K., Bacchi O. O. S & Dias N. M. P. (2008) - *Micromorphological analysis to characterize structure modifications of soil samples submitted to wetting and drying cycles* CATENA, **72**(2): 297-304.

Pourghasemi H.R., Kariminejad N., Gayen A., Komac M. (2019) - *Statistical functions used for spatial modelling due to assessment of landslide distribution and landscape interaction factors in Iran*. Geoscience Frontiers, **11**: 1257-1269. Doi: 10.1016/j.gsf.2019. 11.005

Rezaiy H., Lashkaripour G.R., Ghafoori M. (2011) - *Engineering Geology Criteria for Evaluation and Classification of Loess in Golestan Province*. J. Basic. Appl. Sci. Res., **1**(12): 2979-2986.

Richthofen, F.F. von (1877) - *China. Ergebnisse eigener reisen und darauf gegründeter Studien*. Bd. 1, Einleittender theil Berlin, D. Reimer, 1–758

Romer C. & Ferentinou M. (2016) - *Shallow landslide susceptibility assessment in a semiarid environment a quaternary catchment of KwaZulu-Natal, South Africa.* Engineering Geology, **201**: 29–44.

Salehi T., Shokrian M., Modirrousta A., Khodabandeh M. & Heidari M. (2015) - *Estimation of the collapse potential of loess soils in Golestan Province using neural networks and neuro-fuzzy systems.* Arabian Journal of Geosciences, **8**(11): 9557–9567. Doi: 10.1007/s12517-015-1894-4

Sun P., Peng J., Chen L., Yin Y. & Wu S. (2009) - *Weak tensile characteristics of loess in China An important reason for ground fissures.* Engineering Geology, **108**(1-2): 153–159. Doi:10.1016/j.enggeo.2009.05.014

Vaz T. & Zezere J. L. (2016) - *Landslides and other geomorphologic and hydrologic effects induced by earthquakes in Portugal.* Natural Hazards, **81**:71–98.

Wang G.Y., You G., Shi B., Qiu Z. L., Li H. Y. & Tuck M. (2010) - *Earth fissures in Jiangsu Province, China and geological investigation of Hetang earth fissure.* Environmental Earth Science, **60**: 35–43.

Wang G. Y., You G., Shi B., Yu J., Li H. Y., Zong K. H. (2009) - *Earth fissures triggered by ground-water withdrawal and coupled by geological structures in Jiangsu province, China.* Environmental Geology, **57**: 1047–1054.

Warowna J., Zgłobicki W., Kołodyńska-Gawrysiak R., Gajek G., Gawrysiak L. & Telecka M. (2016) - *Geotourist values of loess geoheritage within the planned Geopark Małopolska Vistula River Gap, E Poland*. Quaternary International, **399**: 46–57. Doi:10.1016/j.quaint.2015.06.064

Xu L., Li S., Cao X., Somerville I.D., Suo Y., Liu X., Dai L., Zhao S., Guo L., Wang P. & Cao H. (2016) - *Holocene intracontinental deformation of the northern North China Plain: evidence of tectonic ground fissures*. J Asian Earth Science, **119**: 49–64.

Xu X., Kalhoro S. A., Chen W., Raza S. (2017) - *The evaluation/application of Hydrus–2D model for simulating macro–pores flow in loess soil* Int. Soil Water Conser. Res., **5**(3): 196-201.

Yalcin A. (2008) - *GIS-based landslide susceptibility mapping using analytical hierarchy process and bivariate statistics in Ardesen (Turkey): comparisons of results and confirmations*. Catena, **72**: 1–12.

Zhang Y., Hu1 Z., Xue Z. (2018) - *A new method of assessing the collapse sensitivity of loess.* Bulletin of Engineering Geology and the Environment, https://doi.org/10.1007/s10064-018-1372-9.

Zizioli D., Meisina C., Valentino R., Montrasio L. (2013) - *Comparison between Different Approaches to Modeling Shallow Landslide Susceptibility: A Case History in Oltrepo Pavese, Northern Italy.* Natural Hazards and Earth System Sciences, **13**(3): 559-573.

Received November 2021 - Accepted May 2022